COMBINATION OF OPTICAL AND MICROWAVE DATA OF ALOS FOR TROPICAL FOREST MAPPING

332

Nguyen Thanh HOAN, Ryutaro TATEISHI

Centre for Environmental Remote Sensing (CEReS), Chiba University,
1-33 Yayoi-cho, Inage-ku, Chiba, 263-6522, Japan
Email: hoanrs@gmail.com

1. INTRODUCTION

Tropical forests cover large parts of the Earth's land surface. These forests hold an enormous biodiversity, and they are disappearing at an alarming rate [1]. Deforestation occurs very quickly in developing countries, the main distribution locations of tropical forests. An example in Vietnam, according to 2005 report conducted by the Food and Agriculture Organization of the United Nations (FAO), Vietnam has the second highest rate of deforestation of primary forests in the world, second only to Nigeria [2]. As of 2005, 12,931,000 hectares (the equivalent of 39.7% of Vietnam's land cover) was forested, although only 85,000 hectares (0.7% of the land cover) was primary forest, the most biodiverse form of forest [3]. Therefore, developing a method of surveying and monitoring tropical forest frequently is very necessary.

Monitoring tropical forest frequently on the ground is very difficult because of complex terrains and expanse of the forest; thus remote sensing images have been widely applied as an important tool for mapping and monitoring forest. Forest mapping by remote sensing data at cover global scale include FRA 2000 by FAO using SPOT Vegetation data, Global Forest Mapping (GRFM/GBFM) Program by JAXA using JERS-1 SAR data. However, the broad categories mapped by these programs fail to deliver valuable and useful information on the variation within the tropical forest environment [4]. Forest mapping using high resolution multi-temporal optical images has been presented in several works e.g. ([4], [5], [6], [7]). But collecting clear high-resolution multi-temporal optical images in tropical regions is very difficult due to the near-daily presence of clouds. The problem is compounded by low temporal resolution of the associated high spatial resolution satellites. Due to its ability to penetrate clouds, microwave remote sensing has proved useful in forest mapping as shown in studies including ([8], [9], [10], [11], [12], [13]). In spite of that, using only microwave data to make a complete forest map has many limitations. The principal uses of radar will be to map forest structure and moisture, this information is largely complementary to that obtained by optical techniques [14]. However, the studies about combination of optical and radar images for forest mapping is not so many, some of them about using synergism of SAR and optical data for land use classification, including some forest types in categories table with limited number of forest classes ([15], [16]). In short, there are some contradictions between spatial resolution and repeat cycle of optical remote sensing data: Optical Moderate Resolution Images (like MODIS, MERIS) have a good repeat cycle, but resolution is too coarse for local studies; on the other hand, Optical High Resolution Images have good resolution, but repeat cycle is too long. Therefore, it is very difficult to separate between Forest and growing Paddy or Cropland because it is not easy to collect multi-temporal data for one year cycle to describe phenology of objects. Microwave data can separate Forest from Crop types and it can be used to analyze structure of forest to complement information for optical data.

ALOS satellite of Japan was launched successfully on January 24 2006. It has both microwave and optical sensor. With high resolution (~10m), this data will be very useful for land studies including forest studies in local scale. The study of combination between optical and microwave data also becomes more feasible. Therefore, this study presents a possibility to improve accuracy of tropical forest mapping by combination of optical and microwave images of ALOS. To support for managing reforestation activities and preserving existing natural forest, discrimination of Planted Forest and Natural Forest is one of the most important purposes of this study. This study will not discuss biomass estimation and wood volume estimation, due to the lack of ground truth measurement data. Cloud removal is a sub-title but it also is an important part of this study.

2. STUDY AREA

The study area, Figure 2.1, is about 6 000 km2 and lies in a tropical zone in the southern part of Vietnam, approximately 50 km north of Ho Chi Minh city, and covers part of Cat Tien national park (one of the biggest natural reserves in Vietnam). The dominant forest in the study area is broadleaf evergreen forest.

Fig. 2.1 Location of the study area (hatched section)

Cat Tien National Park is part of the wet tropical forest complex considered as the reserve of natural resources in Vietnam with lots of rare specious and endemic genes of fauna and flora, and as plentiful site for scientists domestic and foreign tourists. It is one of the specious natural forests remaining in Vietnam.

World Wide Fund for Nature (WWF) International organization has selected Cat Tien National Park as one of the 200 global ecological zones. UNESCO listed the park in 2001 as the 411th biosphere Reserve Zone in the world [17].

3. DATA ACQUISITION AND PREPROCESSING

Four scenes of ALOS/AVNIR-2 and six scenes of ALOS/PALSAR, each set covering the study area, were used in this study. Some more data was also used. All the data is shown in Table 3.1.

Table 3.1 Data used in the study

Data names	Information	Spatial resolution
ALOS AVNIR-2	Four images, date 2007/01/19, 2007/01/19, 2008/02/05, 2007/02/05	10m
ALOS PRISM	Three images in date 2009/03/28, 2009/03/31, 2009/03/31	2.5m
ALOS PALSAR FBS	Six images, three images in date 2007/02/02, the others in date 2007/02/19	6.25m
ALOS PALSAR FBD	Six images, three images in date 2007/06/20 and the others in date 2007/07/07	12.5m
Landsat ETM+	One image, date 2002/01/05	28.5m
Vietnam forest map 2005	Produced in 2008 by Forest Inventory and Planning Institute of Vietnam using Lansat ETM+ images in 2005. It is a newest official forest map of Vietnam in currently	50m
Local map 2005	Nine pieces in vector format, scale 1:50.000, gotten from Map Department, Ministry of Natural Resources and Environment of Vietnam	
SRTM-DEM	The Shuttle Radar Topography Mission 2000 - NASA	90m

3.1. Geometric correction

The ALOS/AVNIR-2, ALOS/PRISM data was bought processed to level 1B2 and ALOS/PALSAR processed to level 1.5, i.e. both data sets were already geo-coded. Nevertheless, features in the two datasets do not coincide. A plane geometric correction method (2-Dimension) was applied to the ALOS/AVNIR-2 images. Ground control points (GCPs) were selected based on local topographic map. For ALOS/PALSAR data, firstly, plane geometric correction using ground control points (GCPs) was used to correct parts that have an elevation of lower than 20m. Then, the corrected ALOS/PALSAR image was corrected further by Orthogonal Geometric Correction method to reduce the effect of terrain. 27 GCPs based on the above corrected ALOS/AVNIR-2 images and a DEM developed from contours of 10m vertical interval (from the topographic map) were used. Used coordinate system is UTM, zone 48, ellipsoid WGS84. Mean errors were constrained less than 1 pixel (10 meters)

3.2. DN value normalization

As shown if Figure 3.1, the left hand side images of the ALOS/AVNIR2 mosaic have an overcast. The mean DN and standard deviation of the overlap for each image were computed and the following linear model [18] was used to normalize the overcast images as shown in equation (1). Mean and standard deviations of two images are shown in Table 3.2 as an example.

Table 3.2 Means and standard deviations of 2 images

Band	Image 1		Image 2	
	Mean	Stdev	Mean	Stdev
Band 1	92	48	69	37
Band 2	73	40	56	33
Band 3	60	36	44	33
Band 4	88	48	89	52

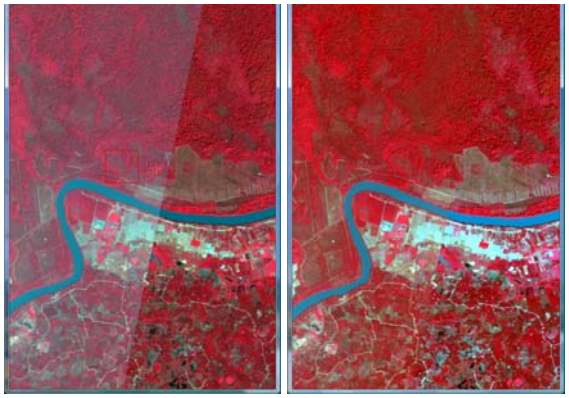

(a) (b)

Fig. 3.1 ALOS/AVNIR-2 mosaic image: (a) before normalization; (b) after normalization. RGB = NIR, Red, Green

$$a[i,j] = (b[i,j] - M_2) * \frac{\sigma_1}{\sigma_2} + M_1 \qquad (1)$$

Where:

M_1, M_2 Mean DN values in clear image and overcast image, respectively

σ_1, σ_2 Standard deviations in clear image and overcast image, respectively

a[i,j] DN value of pixel [i,j] after normalization

b[i,j] DN value of pixel [i,j] before normalization

Figure 3.1(b) shows the normalized mosaic.

In addition, Frost filtering method and window size 5x5 was applied to reduce noise in PALSAR data.

4. CLOUD REMOVAL

Cloud is always problem of optical remote sensing data. And of course, ALOS/AVNIR-2 images are also affected. ALOS/PALSAR data is not affected by cloud. This study proposed a method to remove cloud in optical images based on interpolation from SAR data. Combination of Total Reflectance Radiance Index (TRRI) and Cloud-Soil Index (CSI) is used to define cloud. TRRI is an index developed by Prof. Nguyen Dinh Duong, Vietnamese Academy of Science and Technology (VAST), Vietnam [19] and CSI is an index developed by the author for this study based on some studies before ([20], [21]). Some other technics are used to refine cloud like remove single pixels, extend cloud and so on. Shadow of cloud is also solved by interpolating from cloud based on direction and distance from cloud to shadow. Requirement of this method is suited when objects in ALOS/AVNIR-2 and ALOS/PALSAR data are not different very much. So, this method can apply for the data in which optical image and microwave image in the same geographic place are not very far together about time. With ALOS satellite, it was hoped that this requirement will be satisfied. This method also can be applied for removing cloud from optical images based on other optical images. In this study, some examples of removing cloud in ASTER image based on Landsat/ETM image, removing cloud in Landsat/TM image based on Landsat/TM image are also shown. This method can help to make a series of cloud free multi-temporal images for change detection studies, environment monitoring studies and so on.

4.1. Simulated ALOS data

This study was experimented on simulated ALOS data. ALOS/AVNIR-2 includes 4 spectral channels. Wavelengths of them are close to the first 4 channels of Landsat/TM images. The comparison of both data is shown in Table 4.1.

Table 4.1 Comparison of characteristics between ALOS/ AVNIR-2 and Landsat/TM

Band	ALOS/AVNIR-2	Landsat/TM
1	420 – 500 nm	450 – 520 nm
2	520 – 600 nm	530 – 610 nm
3	610 – 690 nm	630 – 690 nm
4	760 – 890 nm	750 – 900 nm

Therefore, the first 4 bands of Landsat/TM image were used instead of ALOS/AVNIR-2 image.

The frequency of ALOS/PALSAR is close to JERS-1/SAR data (L-band, 1270 MHz and 1300 MHz, respectively). So, JERS-1/SAR data was used instead of ALOS/PALSAR data.

In this study, Landsat/TM image date 1992/10/21 and JERS-1/SAR image date 1992/10/27 of Hanoi, Vietnam were used.

JERS-1/SAR image was resampled to 30 meter spatial resolution to correspond with Landsat/TM image. It was also applied GAMMA 3X3 FILTER ([22], [23]) to reduce noises. And it was corrected about geometry by orthogonal geometric correction before using for interpolation to remove cloud in optical image. The DEM developed from local topographic map 1:50,000 was used for orthogonal geometric correction. Rational Function Math Model of PCI software was used and parameters were computed based on GCPs.

In the Landsat/TM image, there was no cloud. Cloud was gotten from another Landsat/TM image and overlay to Landsat/TM image date 1992/10/21 as shown in Figure 4.1.

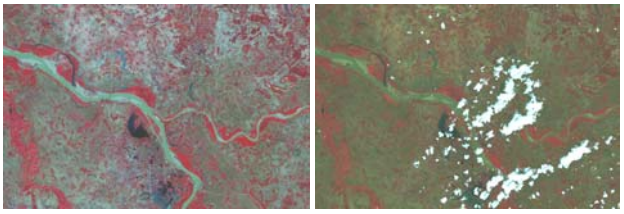

Fig 4.1 Landsat/TM image date 1992/10/21 (left) and after overlaying cloud (right)

By this way, we have perfect data for experimenting the cloud removal program including: cloud image to test the cloud defining method, to test the interpolation method and we also have original data (under cloud data – before overlay cloud) to compare with interpolated result for validation. Figure 3.3 shows the Landsat/TM image after overlaying cloud

4.2. Methodology

Outline of cloud removal methodology is illustrated in Figure 4.2.

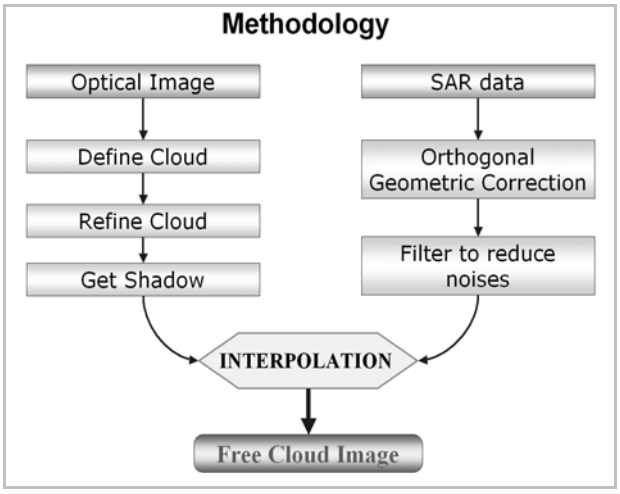

Fig. 4.2 A flow chart of cloud removal methodology

4.2.1. Defining Cloud

Reflectance of cloud is always high from visible wave to near infrared wave. So, values of cloud will be high in the all 4 bands of ALOS/AVNIR-2 data. Therefore, with thick clouds, it is very easy to define them by TRRI index. This index is defined by the equation (2) [19]:

$$TRRI = \frac{\int_{1}^{n} I_i \Delta}{\int_{1}^{n} I_{\max} \Delta} * 100 \qquad (2)$$

Where,

TRRI	Value of index
Ii	Digital count of channel i
n	Number of spectral channels
I_{max}	Maximal digital count for given quantization level
Δ	Spectral channel difference

With thin clouds, they are more difficult. Usually, they are mixed by some dry objects like dry sand or dry bare land. As we know, in the wavelengths from visible to infrared, reflectance of dry bare land is always going up according to growing of wavelength. And reflectance of clear water is always going down ([24], [25]). Because cloud includes water, so reflectance curve of cloud will be going down and reflectance values will be lower in the last bands of ALOS/AVNIR-2 image. The difference of thin cloud reflectance and dry soil reflectance is shown in Figure 4.3 (pixel values were gotten from Landsat/TM image).

To define cloud, the TRRI index is used to divide image into 3 parts: thick cloud, non-cloud and mixture by 2 level values (as shown in Figure 4.3).

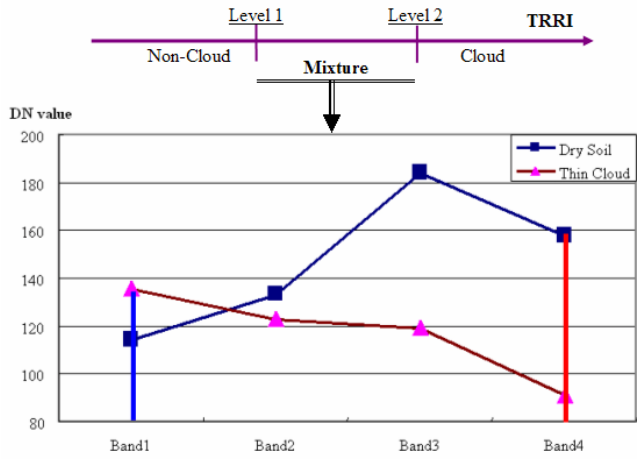

Fig. 4.3 Model for defining cloud

In the mixture part, reflectance of thin cloud in blue band (band 1) is higher than that of dry soil and reflectance of thin cloud in band 4 is lower than that of dry soil. Therefore, thin cloud and other dry objects can be separated by Cloud-Soil Index (CSI). This index is calculated as equation (3).

$$CSI = \frac{Band1 - Band4}{Band1 + Band4} \qquad (3)$$

Based on the model for defining cloud, a program was developed to define cloud by Visual C language. It is called Define Cloud function in a package of programs called Cloud Removal Program. An example result of cloud definition is shown in Figure 4.4.

In this result, boundary of cloud is still white. That is mixture of cloud and other objects, so that is difficult to define. This problem will be solved by extension function in the Refining Cloud section.

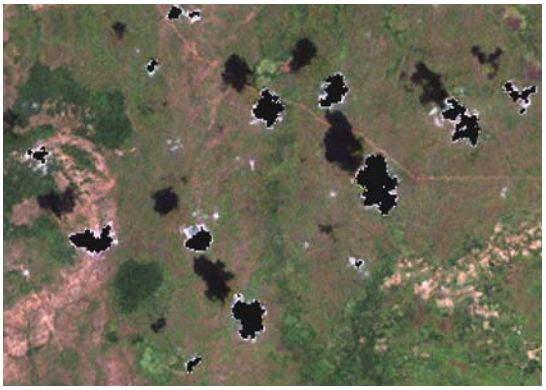

Fig. 4.4 Cloud obtained by the cloud defining method (black areas)

Integrating TRRI index and CSI index can separate cloud and non-cloud quite well. This model can apply for every type of multi-spectral optical image.

4.2.2. Refining Cloud

The Clouds after defining still has some mistakes. Single pixels exist in some places. These pixels were estimated by visually that are some dry objects like buildings and something like that. To correct these mistakes, a function was developed to remove the single pixels. After defining cloud, if result has some single pixels, this Remove Single Pixels function can be used to make a better result.

The around-cloud pixels are mixture of cloud and other objects. So, that is very difficult to define. In this study, the around-cloud pixels are extended from cloud. Another individual function was developed for this purpose. By this extension function, the cloud after defining can be extended to cover all real cloud. An example result of this function is shown in Figure 4.5 (b).

4.2.3. Extraction of shadow

Shadow is always difficult problem. Shadows of clouds on the different objects will have different values. Therefore they are very difficult to define. In this study, shadows are interpolated from clouds. For each image, average distance from clouds to their shadows is determined. Direction of shadow is also estimated. Based on these parameters, a function was developed to interpolate shadows from clouds. An example result is shown in Figure 4.5(a) (black is cloud and brown is shadow)

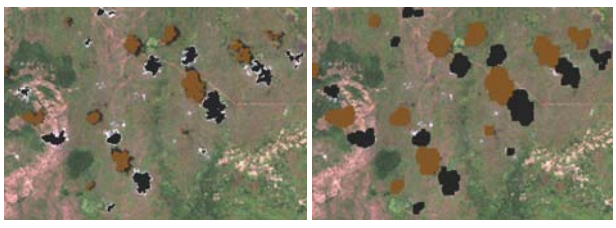

(a) (b)

Fig. 4.5 (a) Interpolated Shadows from Cloud; (b) Clouds and Shadows after extension

Normally, clouds are in different heights. Elevations of terrain under shadows are also different. So, distance from clouds to shadows will be not constant. In this function, average distance is used and of course it will be not a perfect distance. Therefore, interpolated shadow does not cover whole real shadow. After interpolating, shadow result will be extended to cover all real shadow of cloud. Cloud and Shadow after extension is shown in Figure 4.5(b)

4.2.4. Interpolating to remove cloud

To remove clouds and shadows, pixel values of clouds and shadows will be replaced by new values. These new values are interpolated from radar image. An interpolation function was developed to describe this algorithm.

With each cloud or shadow pixel in optical image, the interpolation function will find the corresponsive pixel (same location pixel) in radar image and get DN value of this pixel in the radar image. Then, the function will search from the nearest pixels to farther pixels in the radar image to find a similar pixel with the centre pixel. When meet the pixel that satisfy the condition as the equation (4) and it is not cloud or shadow in optical image, the searching will be stopped.

$$abs(DN_i - DN_j) \le a \qquad (4)$$

Where,

a	is threshold value
DN_i	is digital number of centre pixel
DN_j	is digital number of searching pixel

From DN_j position, program will find in the reverse direction to corresponsive pixel in the optical image. Then, DN value in this position will be gotten to replace for cloud or shadow pixel in the central position of searching window. Processing will be done one pixel by one pixel. The schematic image of this algorithm is described in Figure 4.6.

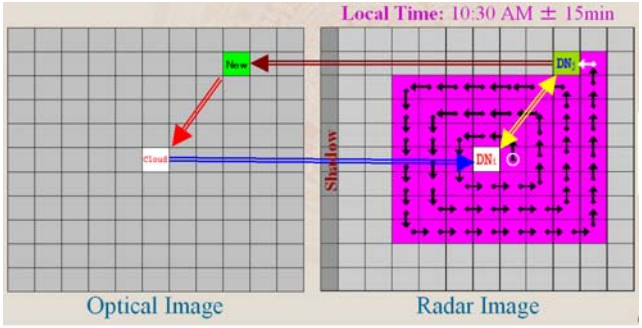

Fig. 4.6 Interpolation model to remove cloud

Local time of ALOS satellite is 10:30 am ± 15 minutes. It means that the sun will be in the right side of image and shadow will be in the left side of image. To reduce effects of shadow, interpolation will be started from right-down pixel of each distance. This interpolation is illustrated by arrows in Figure 4.6. The white circle is started pixel of interpolation.

As we know, optical data and microwave data are very different together. The same values in microwave data do not guarantee that values in optical data will be the same. However, if the pixels are near together, likelihood of the same objects in optical data will be higher because the same objects are usually distributed in the same geographic regions. So, result image will have more information than cloud image and microwave image if using them independently.

In addition, some other functions were developed to support for image processing like Mask Cloud function and Change Code function.

4.3. Experiments

The Cloud Removal Program will be experimented on the simulated ALOS data, ASTER data, Landsat/ETM data, and finally applied for real ALOS data. These experiment results will be presented in the next sections.

4.3.1. On simulated ALOS data

Result is a cloud free and shadow free image. Interpolated image is compared with the original image (before overlaid by cloud) by visually. Interpolated image and original image look very similar together as shown in Figure 4.7.

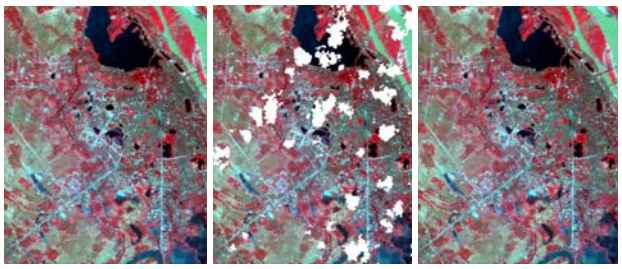

(a) (b) (c)

Fig. 4.7 Comparison of original and interpolated image; (a) Original image, (b) Cloud image, and (c) Interpolated image

However, some objects in some parts have some mistakes. Comparison of red object (inside the yellow circle in Figure 4.8) in interpolated image and original image is not the same together. Shape of these objects in original image is very clear, but shape of them in interpolated image is not clear. This problem is shown in Figure 4.8.

This object was checked in radar image but that cannot be determined by radar image from around objects. This problem may be because of radar image (backscatter is the same with around objects) or change of the object (radar image and optical image are different 6 days). This checking is illustrated in Figure 4.8.

These objects were already confirmed by local native farmers. That is one type of vegetable. Height of this vegetable is about 20-30cm. It covers nearly 100% of land. Maybe, it looks like a flat surface by radar L-band.

In Figure 4.8, the big vegetable fields can be seen very clearly in the left-top corner of optical image (red color), but they cannot be determined by JERS-1/SAR images. Therefore, cause of radar image (can not separate this object by radar image) is higher probability than cause of change of object. So, interpolation of under cloud data based on radar image will be not so good at some special objects like that. However, by using combination of threshold level (a value) for radar image and searching the nearest pixel to interpolate cloud pixel, the result will have more information than using threshold of whole radar image and cloud optical image independently.

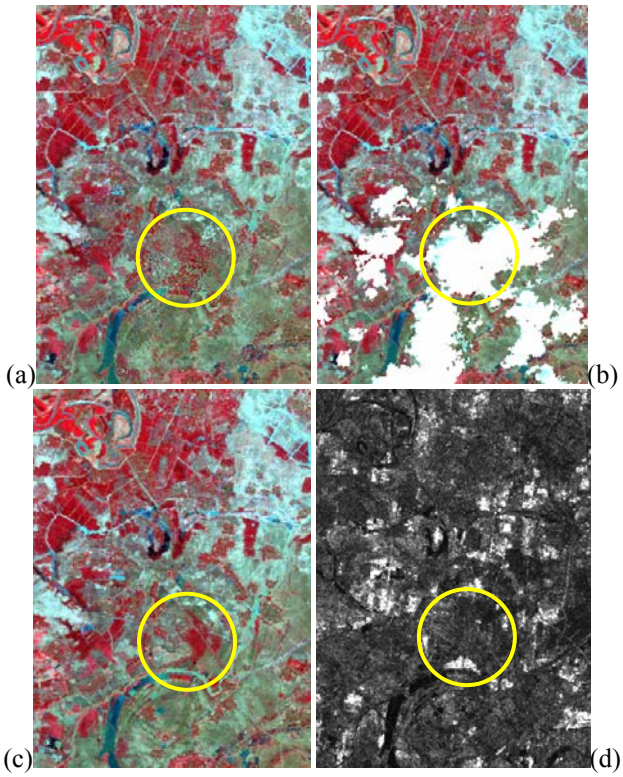

(a) (b) (c) (d)

Fig 4.8 Problems of interpolated image; (a) Interpolated image, (b) Cloud image, (c) Original optical image, and (d) radar image

4.3.2. Cloud removal of ASTER image based on Landsat/ ETM image

This Cloud Removal program also can be applied for combination of two optical images to remove cloud if the change of objects is not so much. By the same way, cloud was gotten from another image to overlay on ASTER image date 2001/11/16. The NDVI of Landsat/ETM image date 2000/11/04 was used instead of radar image. Interpolated image is compared with original image by visually. Result is very good. Almost there are no change between interpolated result and original ASTER image. An illustration result is shown in Figure 4.9.

By this way, many types of different optical images can be combined together to remove cloud. It can be used to make a series of cloud free multi-temporal data from

many types of satellite data for studies about monitoring the change in environment and natural resource.

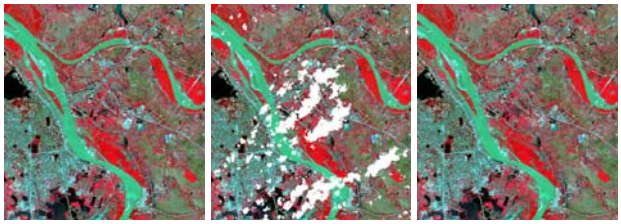

(a) (b) (c)

Fig. 4.9 Removing Cloud of ASTER image date 2001/11/16; (a) Original image, (b) Cloud image, and (c) Interpolated image

4.3.3. Combination of two Landsat/ETM images

Here is another application of the Cloud Removal Program. Two Landsat/ETM images date 2002/01/05 and 2001/02/03 were used. Both of them have clouds. These two images can be combined together to make two cloud free images. In this case, wavelengths of two images are the same together. So, interpolation is done based on band by band. That means using band 1 to interpolate for band 1, band 2 to interpolate for band 2, band 3 to interpolate for band 3 and so on. The first, cloud parts in the image date 2001/02/03 were removed based on the image date 2002/01/05. The result is shown in Figure 4.10.

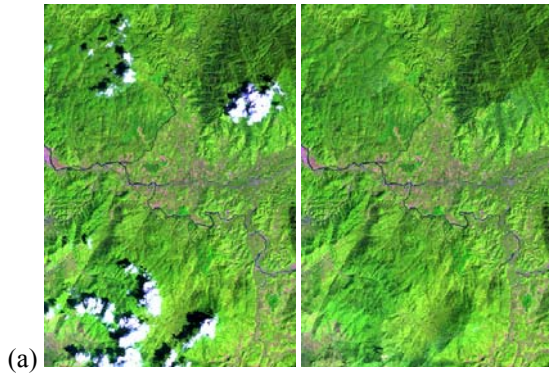

(a) (b)

Fig. 4.10 Removing cloud from Landsat/ETM image on 2001/02/03; (a) Cloud image and (b) interpolated image

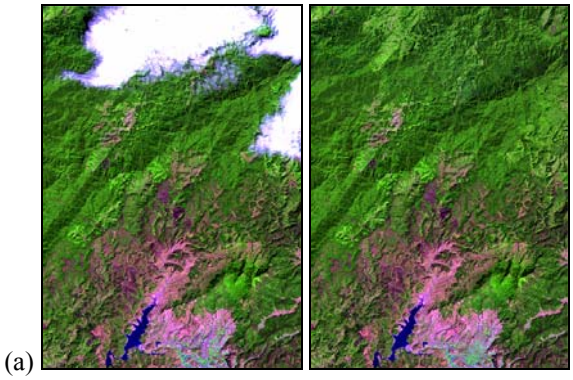

(a) (b)

Fig. 4.11 Removing cloud from Landsat/ETM image on 2002/01/05; (a) Cloud image and (b) interpolated image

By the same way, cloud parts in the image date 2002/01/05 were removed based on the image date 2001/02/03. The result is shown in Figure 4.11.

Result shows as two cloud free images. These images are really perfect results. Every object in the interpolated images looks very natural and logical. If spatial change of objects covered by cloud is not so much, this method is perfect way for removing cloud to make a multi-temporal dataset for one type of data or for the types of data that have similar wavelengths.

4.3.4. Applying the Cloud Removal Program on real ALOS data

ALOS/PALSAR FBS image after applying FROST filtering method, window size 5x5 was used to remove clouds from ALOS/AVNIR-2 image. Result is a cloud free and shadow free image. As a whole, result is good. The under cloud pixels after interpolation look smooth and natural by visually. More detail, some parts were zoomed in and checked by classification result. In Figure 4.12, the main objects covered by clouds and shadows are forests and some water. These objects look good in the interpolated image (after cloud removal) and in classification result.

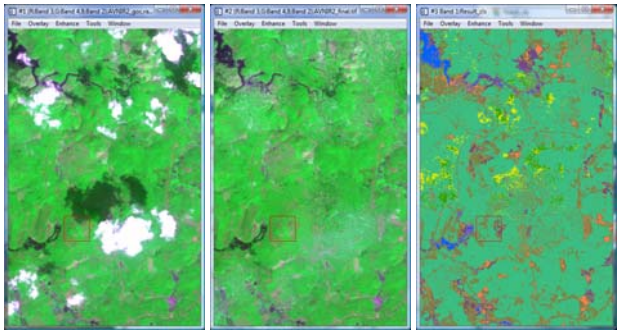

(a) (b) (c)

Fig. 4.12 Water and forest in cloud removal result of ALOS/AVNIR-2 image, (a) before cloud removal (RGB: Red, NIR, Green), (b) after cloud removal, and (c) classification result

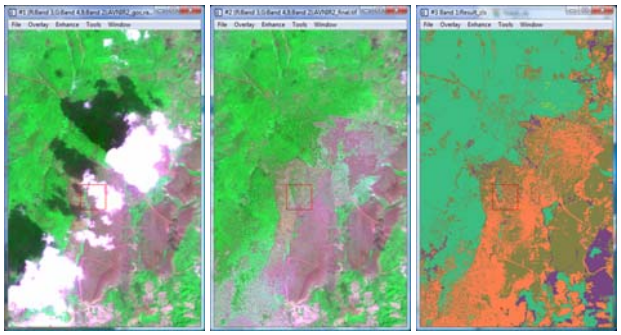

(a) (b) (c)

Fig. 4.13 Cropland and forest in cloud removal result of ALOS/AVNIR-2 image, (a) before cloud removal (RGB: Red, NIR, Green), (b) after cloud removal, and (c) classification result

In Figure 4.13, main objects covered by clouds and shadows are forest, some croplands and grass lands. The result looks good at the center part of the image (that is boundary of forest and grass land). But it looks not very good at the place that is boundary of cropland and grass land (the clouds in the left-bottom corner of Figure 4.13). This situation is the same as the problem presented in the section 4.3.1 - Figure 4.8 - because the radar image L band cannot separate some types of land cover like cropland, grass land and bare land together. Therefore, cloud removal result should be not good at the parts that are boundaries of those objects.

4.4. Conclusions

Combination of TRRI index and CSI index to define cloud showed a good result. This method can be applied for every multi-spectral optical image to extract cloud.

Shadow interpolated from cloud will be larger than real shadow. It is one of limitations of the Cloud Removal Program

Result image after removing cloud based on radar image is good, no cloud and shadow. Distribution of objects under cloud and shadow after interpolation processing almost is good, smooth and natural by visually. However, some parts are not so good after interpolation if they are boundaries between some objects that cannot be separated together from PALSAR data like cropland, grassland and bare land.

Combination of two optical images to remove cloud is good way to make cloud free multi-temporal dataset. Condition to apply this method is satisfied when the change of objects that covered by clouds and shadows are not so much.

Final result of this section is a program with many functions like: define cloud, extend cloud, get shadow, remove cloud and so on. This is free software for every user.

5. TROPICAL FOREST MAPPING

For the study area, in the year 2007, only a one-time acquisition of ALOS/AVNIR-2 images were clear enough for the cloud removal described in § 4. These images are not adequate to describe phenology of forest. The following sections will present a proposal to combine single-temporal ALOS/AVNIR-2 images and multi-temporal ALOS/PALSAR images for tropical forest mapping.

The ALOS/AVNIR-2 mosaic image was pan-sharpened to 2.5m using the ALOS/PRISM mosaic image. The 11 land-covers given in Table 5.1 were visually identifiable in the pan-sharpened ALOS/PRISM image. National Forest Inventory - Field Manual [26], the Forest Vegetation of Vietnam [27] and the Vietnam Forest Map 2005 aided in the visual interpretation. As the table shows, there are five classes of forest in the study area.

Table 5.1 Forest types within Cat Tien national park and surrounding areas, in southern part of Vietnam.

Class name	Description
1. Primary forest	Undisturbed Broad-leaf evergreen and semi-deciduous forest stands. Canopy closure is more than 60% by high trees
2. Degraded forest	Forest areas with a considerable human distbuilt-up areace. These areas might include forest growing back from clear-felling, resulting from either shifting cultivation of logging (secondary forest) or areas affected by pronounced selective logging. Canopy of high trees is usually small and canopy closure of high trees is less than 30%
3. Bamboo	Areas dominated by bamboo. The term bamboo refers to old, naturally occurring bamboo areas as well as to second growth bamboo following clear-felling.
4. Mixed forest	Mixture of high trees, bamboo and shrubs. These areas are almost affected by selective logging. Canopy of trees is still big but sparse. Canopy coverage of high trees is about from 30-60%
5. Planted forest	The forest is planted by reforestation projects, rubber forest and so on
6. Shrub & Grass	Areas dominated by shrub, bushes or grass reaching a height less than 5m.
7. Mosaic	Mixture of natural vegetation and cropland, or family gardens
8. Paddy/Crop land	Paddy fields or croplands
9. Built-up area	Built-up area, high density residential areas or built-up areas
10. Wetland	Swamps covered by some types of herbaceous
11. Water	Water bodies

5.1. Advantages and disadvantages of AVNIR-2 data for tropical forest mapping

To determine ability of ALOS/AVNIR-2 images for tropical forest mapping, K-mean classification was executed on the ALOS/AVNIR-2 mosaic and the resultant spectral classes labeled in relation to the above information classes based on PRISM-sharpen image. Main clear classes will be used as training data for supervised classification - Maximum Likelihood method. Table 5.2 shows error matrix of the classification result (using validation data as shown in §5.4). Result shows that using only single-temporal image of AVNIR-2 can

separate well between Forest, Shrub & Grass, Wetland, Water and so on, but it is very difficult to separate between Planted forest and Natural forest, between Forest and growing Paddy/Cropland, between Built-up area and some other land cover types.

Table 5.2 Error matrix of classification result of ALOS/AVNIR-2 mosaic image

	Reference data											∑	%
Cls	[1]	[2]	[3]	[4]	[5]	[6]	[7]	[8]	[9]	[10]	[11]		
[1]	11	0	0	1	0	0	0	0	0	0	0	12	**92**
[2]	1	37	2	4	3	0	0	0	0	0	0	47	**79**
[3]	0	1	5	2	2	0	0	0	0	0	0	10	**50**
[4]	1	1	0	25	2	0	0	0	0	0	0	29	**86**
[5]	1	2	3	4	72	0	5	13	0	0	0	100	**72**
[6]	0	0	0	0	0	43	4	0	2	0	0	49	**88**
[7]	0	0	0	0	0	7	40	0	2	0	0	49	**82**
[8]	0	0	0	0	0	0	0	0	0	0	0	0	**0**
[9]	0	0	0	0	0	0	0	0	0	0	0	0	**0**
[10]	0	0	0	0	2	0	9	2	0	5	0	18	**28**
[11]	0	0	0	0	0	0	0	0	0	0	16	16	**100**
∑	14	41	10	36	81	50	58	15	4	5	16	330	
%	**79**	**90**	**50**	**69**	**89**	**86**	**69**	**0**	**0**	**100**	**100**		

Number [1] is order of class name as shown in Table 5.1

Overall accuracy is 77% and Kappa coefficient is 0.73.

ALOS/PALSAR data will be used to improve accuracy of this map.

5.2. Advantages of PALSAR data for tropical forest mapping

Radar remote sensing is vital for monitoring forest because it provides information on canopy volume. Secondly, RADAR is not affected by clouds and haze associated with the tropics [28]. In this study, radar data was used for to discriminate between forests and growing paddy/cropland that cannot be separated by ALOS/AVNIR-2 optical image (as shown in §5.1), as well as discriminating between planted forest and natural forest by analyzing forest structure.

According to Alvin Wong [29], there are four main scattering mechanisms of radar including: “Smooth Surface”, “Rough Surface”, “Double-bounce”, and “Vegetation layers”. Where "Smooth Surface" backscattering is the weakest and "Double-bounce" scattering is the strongest. These scattering mechanisms will be used to analyze the differences in objects of interest in the next sections.

5.2.1. Discrimination of Planted forest and Natural forest

The main difference between tropical planted forest and tropical natural forest is their structures. Tropical planted forest normally has only one layer of trees and the density of the trees is usually not very high. Tropical natural forest always has more than one layer of trees, usually with very high density of the trees and many branches and lianas. According to Thuy Le Toan [28], the main scatterers of tropical natural forest are as shown in Table 5.3.

Table 5.3 Main scatterers in tropical natural forest

Frequency band	X	C	L	P	VHF
Main scatterers	Leaves, Twigs	Leaves, Small branches	Branches	Branches & Trunk	Trunk

Using ALOS/PALSAR (L-band), in forest, the scattering is affected mainly by branches of tree. The number of branches is one of the main differences between tropical planted forest and tropical natural forest. Thus tropical planted forest and tropical natural forest can be discriminated by ALOS/PALSAR images in theory.

Based on the scattering mechanisms, backscatter of tropical natural forest with many branches and lianas is mainly by "vegetation layer". Backscatter of tropical planted forest should be stronger with a significant amount of the "double-bounce" scattering mechanism because some radar signals can go through the forest canopy to the ground and be backscattered by the ground and trunks.

As Figure 5.1(a) shows, planted and natural forest cannot be differentiated visually in an AVNIR-2 image. However, they can be in PALSAR images (Figure 5.1b and 5.1c). In the PALSAR images, natural forest looks darker and planted forest looks lighter. The difference between the two types of forests is clearer in the HH polarization image than in the HV polarization image. In this study, both polarization HH and HV were used to separate between planted forest and natural forest.

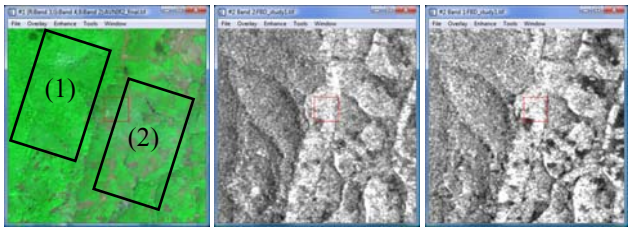

(a) (b) (c)

Fig. 5.1 Natural forest (1) and plantation forest (2) in; (a) AVNIR-2 images, (b) PALSAR HH-polarization image, and (c) PALSAR HV-polarization image

FROST filtering method with a window size of 15x15 ([22], [23]) was applied on the HH- and HV-polarized images. The images were then clustered into 20 spectral classes by K-mean classification method. The spectral classes were labeled into natural and non-natural forest. Post-classification smoothing was then carried out. This result called natural forest mask will be used in a combination model to make final forest map (§5.3).

5.2.2. Discrimination between forests and growing paddy/croplands/built-up areas

Paddy/cropland appears as smooth surface in the L band of ALOS/PALSAR in any season [30]. Backscattering of

forest is defined by "Vegetation layer" and "Double-bounce" scattering mechanisms as presented in §5.2.1. Therefore, backscattering of forests should be higher than that of paddy/croplands. In this study, ALOS/PALSAR single-polarized (HH) images were used to form the paddy/cropland mask. Level slicing method was applied to divide the PALSAR images into four layers including: water and no-data, paddy/croplands, built-up area, and others.

The paddy/cropland and built-up layers will be used as masks in a combination model to make the final forest map.

5.3. Combination model

The result classified from ALOS/AVNIR-2 images was used as a background image to combine with the natural forest mask, paddy/cropland mask and built-up mask derived from ALOS/PALSAR images for producing the final tropical forest map. This combination was summarized in one combination model as shown in Figure 5.2.

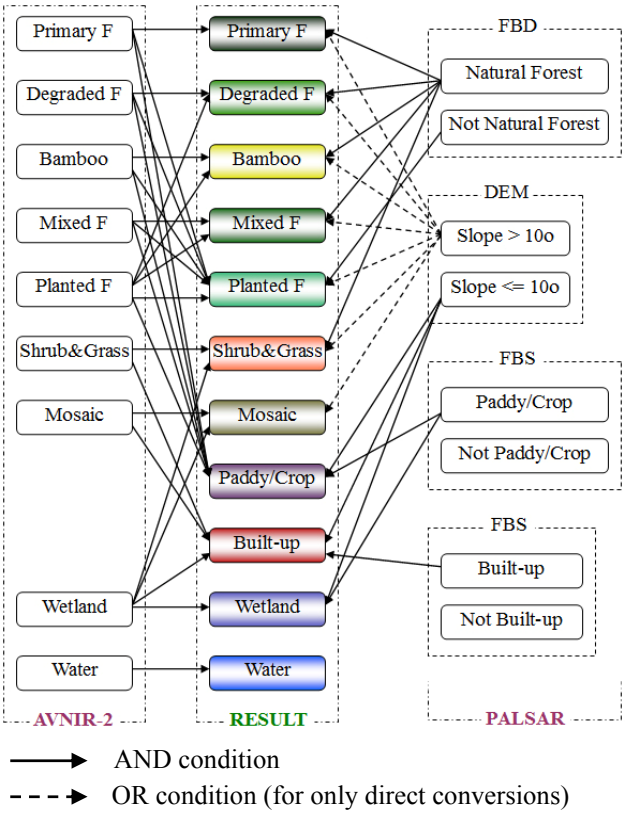

Fig. 5.2 The combination model of AVNIR-2 and PALSAR images for tropical forest mapping

Where, the left box is the classified result from AVNIR-2 image; the right box is results (masks) obtained from PALSAR analysis and the center box is combination result.

According to Feilong Ling [9], multi-temporal ALOS/PALSAR dual-polarization data can create accurate maps for forest in flat areas. The capability to map forest in hilly regions is still limited. Furthermore, the analyses in this study showed a similar result. Therefore, the slope map developed from the 10m resolution DEM was used to correct for slope areas. In this model, the areas that have slope higher than 10^{o} will be kept as ALOS/AVNIR-2 classification result.

In the Figure 5.2, the continuous vectors present for AND condition. That means, the parameters at begin of the vectors will be used AND function to combine with other parameters. The dashed vectors present for OR condition. The parameters at begin of the vectors will be used OR function to combine with other parameters. The dashed vectors will be used in direct conversions only. That means, the parameters at begin of the vectors will be used to combine with other parameters only when destination has the same class name with original class, e.g. converting from Primary F of AVNIR-2 box to Primary F of RESULT box, from Bamboo of AVNIR-2 box to Bamboo of RESULT box, and so on.

One example to explain the combination model, from original Primary Forest as shown in the box of AVNIR-2 will have three destinations presented in the RESULT box: to Primary F when the pixel is in natural forest mask OR slope is higher than 10^{o}; to Planted F when the pixel is not in natural forest mask; and to Paddy/Crop when the pixel is in paddy/crop mask AND slope is lower or equal 10^{o}. The order of priority functions is from up to down. Other classes were done by similar ways. Figure 5.3 shows the final tropical forest map.

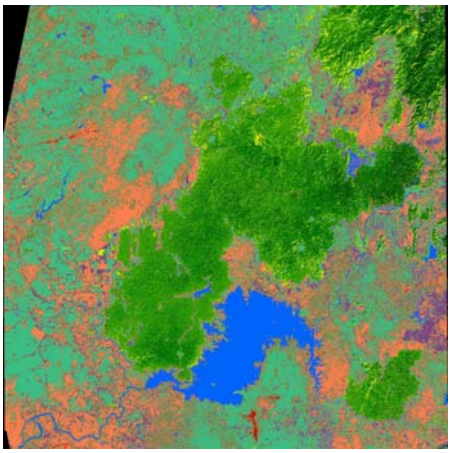

Fig. 5.3 Final tropical forest map 2007

5.4. Accuracy assessment

330 random pixels, Figure 5.4, from ALOS/AVNIR-2 mosaic were selected to validate the 11 land-covers in Table 5.1. An average of 30 pixels was used for each land-cover type. The resultant error matrices are shown in Tables 5.2 and 5.4. Before combination, the overall accuracy was 77% and Kappa coefficient was 0.73. After combination the overall accuracy increased to 88% and Kappa coefficient was 0.86.

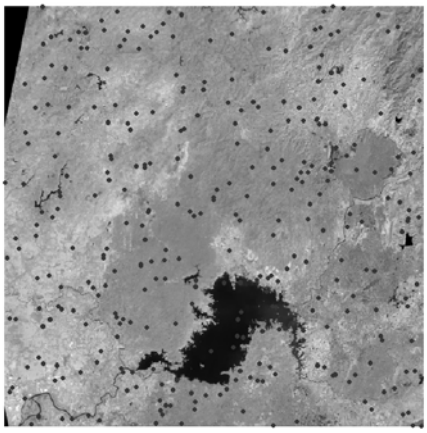

Fig. 5.4 Distribution of 330 random points for validation

Table 5.4 Error matrix of combination result between ALOS/AVNIR-2 and ALOS/PALSAR images

	Reference data											∑	%
Cls	[1]	[2]	[3]	[4]	[5]	[6]	[7]	[8]	[9]	[10]	[11]		
[1]	11	0	0	1	0	0	0	0	0	0	0	12	**92**
[2]	1	38	0	4	0	0	0	0	0	0	0	43	**88**
[3]	0	1	8	2	0	0	0	0	0	0	0	11	**73**
[4]	2	2	0	28	0	0	0	0	0	0	0	32	**88**
[5]	0	0	2	1	77	0	4	0	0	0	0	84	**92**
[6]	0	0	0	0	0	43	4	0	0	0	0	47	**92**
[7]	0	0	0	0	2	7	48	0	0	0	0	57	**84**
[8]	0	0	0	0	2	0	1	13	0	0	0	16	**81**
[9]	0	0	0	0	0	0	0	0	4	0	0	4	**100**
[10]	0	0	0	0	0	0	1	2	0	5	0	8	**63**
[11]	0	0	0	0	0	0	0	0	0	0	16	16	**100**
∑	14	41	10	36	81	50	58	15	4	5	16	330	
%	**79**	**93**	**80**	**78**	**95**	**86**	**83**	**87**	**100**	**100**	**100**		

Number [1] is order of class name as shown in Table 5.1

Overall accuracy is 88% and Kappa coefficient is 0.86.

Primary forest, Degraded forest and Mixed forest are natural forests, Sometimes it is very difficult to distinguish between them even by visual interpretation using very high resolution images like PRISM pan-sharpened images. For forest management purposes, they could be merged into one natural forest class only. In this case, it is also noteworthy that the user's and producer's accuracies of the main forest types increased in the proposed method, as shown in Table 5.5. The overall accuracy increased from 87% to 95%. All the categories of accuracies of natural forest and planted forests became higher after combination of ALOS/AVNIR-2 classification result and ALOS/PALSAR analysis results.

Table 5.5 Accuracies of main forest classes before and after combination

	User's accuracy		Producer's accuracy	
Classified	Before	After	Before	After
Natural forest	92%	100%	89%	96%
Planted forest	72%	92%	89%	95%
Bamboo	50%	73%	50%	80%

Overall accuracy before the combination	87%
Overall accuracy after the combination	95%

5.5. Conclusion

Using single-temporal optical data like ALOS/AVNIR-2 is not adequate to separate between forests and growing paddy/croplands and built-up areas, between planted forests and natural forests. However, using PALSAR single-polarized image is easy to discriminate between forests and growing paddy/croplands, between built-up and others. On the other hand, using PALSAR dual-polarized images can separate between planted forests and natural forests, however not very perfect.

Combination of single-temporal image of AVNIR-2 and multi-temporal images of PALSAR for tropical forest mapping is a feasible way for every year. Tropical forest mapping annually by high resolution images becomes possible with ALOS data.

Combination of optical and microwave data of ALOS by a combination model can improve accuracy of tropical forest mapping. The accuracy was increased up so much after the combination. The final tropical forest map has a high accuracy, especially for main forest classes.

6. REFERENCES

[1] NUGROHO, M., "Integration of Multi Remotely Sensed Data and Geodatabases for Forestry Management in Indonesia". PhD thesis, Wageningen University, The Netherlands, 2006.

[2] BUTLER and RHETT, A., "Nigeria has worst deforestation rate", FAO revises Figures, 2005. Available online at: Mongabay.com (accessed 14 September 2009).

[3] MEYFROIDT, P., LAMBIN, E.F., "Forest transition in Vietnam and its environmental impacts". *Global Change Biology*, 14 (6), pp. 1319-1336, 2008.

[4] TOTTRUP, C., "Improving tropical forest mapping using multi-date Landsat TM data and pre-classification image smoothing". *International Journal of Remote Sensing*, 25, pp. 717-730, 2004.

[5] RAHMAN, M.M., CSAPLOVICS, E., KOCH, B., "An efficient regression strategy for extracting forest biomass information from satellite sensor data". *International Journal of Remote Sensing*, 26, 1511-1519, 2005.

[6] FOODY, G.M., BOYD, D.S., CUTLER, M.E.J., "Predictive relations of tropical forest biomass from Landsat TM data and their transferability between regions". *Remote Sensing of Environment*, 85, 463-474, 2003.

[7] HELMER, E.H., BROWN, S., COHEN, W.B., "Mapping montane tropical forest successional stage and land use with multi-date Landsat imagery". *International Journal of Remote Sensing*, **21**, pp. 2163-2183, 2000.

[8] ALMEIDA-FILHO, R., SHIMABUKURO, Y.E., ROSENQVIST, A., SANCHEZ, G.A., "Using dual-polarized ALOS PALSAR data for detecting new fronts of deforestation in the Brazillian Amazonia". *International Journal of Remote Sensing*, **30**, pp. 3735-3743, 2009.
[9] LING, F., LI, Z., CHEN, E., WANG, Q., "Forest mapping with multi-temporal dual polarization ALOS PALSAR data". *Procedings of SPIE*, Vol. 7285, 728517 (2008).
[10] CLOUDE, S., VIERGERVER, K., WOODHOUSE, I.H., "Forest Stucture Estimation using POLInSAR". CD *Proceedings of the first joint PI symposium of ALOS data nodes for ALOS science program in Kyoto*, JAXA, Nov. 2007.
[11] FRANSSON, J.E.S., MAGNUSSON, M., OLSSON, H., ERIKSSON, L.E.B., SANDBERG, G., SMITH-JONFORSEN, G., ULANDER, L.M.H., "Detection of forest changes using ALOS PALSAR satellite images". *CD Proceedings of Geoscience and Remote Sensing Symposim (IGARSS)*, Barcelona, July 23-27, 2007.
[12] SGRENZAROLI, M., DE-GRANDI, G.F., EVA, H., ACHARD, F., "Tropical forest cover monitoring estimates from the GRFM JERS-1 radar mosaics using wavelet zooming techniques and validation". *International Journal of Remote Sensing*, 23, pp. 1329-1355, 2002.
[13] TAKEUCHI, S., SUGA, Y., OGURO, Y., KONISHI, T., "Monitoring of new plantation development in tropical rain forests using JERS-1 SAR data". *Advances in Space Research*, 26, pp. 1151-1154, 2000.
[14] DOBSON and CRAIG, M., "Forest information from Synthetic Aperture Radar". *Journal of Forestry*, 98, pp. 41-43, 2000.
[15] KUPLICH, T.M., "The study of ERS-1 SAR and Landsat TM synergism for land use classification". *International Journal of Remote Sensing*, **21**, pp. 2101-2111, 2000.
[16] HYYPPA, J., HYYPPA, H., INKINEN, M., ENGDAHL, M., LINKO, S., ZHU, Y.H., "Accuracy comparison of various remote sensing data sources in the retrieval of forest and attributes". *Forest Ecology and Management*, 128, pp. 109-120, 2000.
[17] UNESCO, "Tentative lists - World Heritage Centre", 2009. Available online at:
http://whc.unesco.org/en/tentativelists/5070/ (accessed 20 September 2009).
[18] DUONG, N.D., THOA, L.K., HOAN, N.T., BINH, C.T., "Monitoring of Forest Cover Change in Tanh Linh District, Binh Thuan province, Vietnam by Multi-temporal Landsat". *Proceedings of the 20th Asian Conference on Remote Sensing*, Vol.1, pp.260-265, Nov. 1999.
[19] DUONG, N.D., "Total Reflected Radiance Index – An Index to Support Land Cover Classification". P*roceedings of the 19th Asian Conference on Remote Sensing*, Manila, Philippines, pp. H-7-1 to H-7-6, Nov. 2008.
[20] HOAN, N.T., DUONG, N.D., "Proposing a Method to Establish Vietnam Forest Map by Using Multi-temporal GLI Images and Ecologic Models". *Proceedings Japan-Vietnam Geoinformatics Consortium Symposium*, Hanoi, Vietnam, CH1, pp. 457-463, 2004.
[21] HOAN, N.T., DUONG, N.D., TATEISHI, R., "Combination of ADEOS II – GLI and MODIS 250m Data for Land Cover Mapping of Indochina Peninsula". CD *Proceedings of the 26th Asian Conference on Remote Sensing (ACRS)*, Hanoi, Vietnam, LLC1-2, Nov. 2005.
[22] LOPES, A., NEZRY, E., TOUZI, R., AND LAUR, H., "Structure detection and statistical adaptive speckle filtering in SAR images". *International Journal of Remote Sensing*, 14, pp. 1735-1758, 1993.
[23] ZHENGHAO, S. AND FUNG, K.B., "A Comparison of Digital Speckle Filters". *Proceedings of International Geoscience and Remote Sensing Symposium (IGARSS 94)*, pp. 2129-2133, 1994.
[24] MURAI, S., "Remote Sensing Note". Published by Japan Association on Remote Sensing, Tokyo, Japan, pp.18-19, 1996.
[25] LIEW, S.C., "Principles of Remote Sensing (digital book)". Centre for Remote Imaging, Sensing and Processing, National University of Singapore, 2001.
[26] FAO (Food and Agriculture Organization), "National Forest Inventory - Field Manual Template". Forestry Department, FAO, 2004. Available online at: http://www.fao.org/documents/pub_dett.asp?pub_id=191385&lang=en (accessed 29 August 2009).
[27] VIETNAMESE, TRUNG, T.V., "Thảm thực vật rừng Việt Nam, N.T. HOAN (The forest vegetation of Vietnam)". Science and Techniques Publishing House, Hanoi 1997, pp. 197-243, 1997.
[28] TOAN, T.L., PICARD, G., MARTINEZ, J.M., MELON, P., DAVIDSON, M., "On the relationships between RADAR measurements and forest structure and biomass". *CD Proceedings of the 3rd International Symposium, "Retrieval of Bio- and Geophysical Parameters from SAR Data for Land Applications"*, Sheffield, UK, Sep. 2001.
[29] WONG, A., CHAPMAN, B., RICHARDSON, A., FREEMAN, A., "SIR-C EDucation #03 (SIRCED03-B)" CD-ROM, PC Special Edition, California Institute of Technology, Pasadena, California, USA, 1997.
Available online at:
http://southport.jpl.nasa.gov/cdrom/sirced03/cdrom/DOCUMENT/HTML/TEACHERS/MODULE02/MOD2SECE.HTM (accessed 10 September 2009)
[30] ISHITSUKA, N., "The scatter characteristic of rice paddy fields using L band multi polarimetric satellite SAR observation". *CD Proceedings of the first joint PI symposium of ALOS data nodes for ALOS science program in Kyoto*, JAXA, Nov. 2007.